A hierarchical lattice structure and formation mechanism of ZnO nano-tetrapods

2009 Nanotechnology 20 325709

(http://iopscience.iop.org/0957-4484/20/32/325709)

Nanotechnology **20** (2009) 325709 (6pp) doi:10.1088/0957-4484/20/32/325709

A hierarchical lattice structure and formation mechanism of ZnO nano-tetrapods

Yaping Wu[1], Xian-Hua Zhang[1,2], Fuchun Xu[1], Lan-Sun Zheng[2] and Junyong Kang[1,3]

[1] Fujian Key Laboratory of Semiconductor Materials and Applications, Department of Physics, Xiamen University, Xiamen 361005, People's Republic of China
[2] State Key Laboratory for Physical Chemistry of Solid Surfaces, Department of Chemistry, Xiamen University, Xiamen 361005, People's Republic of China

E-mail: jykang@xmu.edu.cn

Received 29 March 2009, in final form 26 June 2009
Published 21 July 2009
Online at stacks.iop.org/Nano/20/325709

Abstract

The existence of characteristic longitudinal optical and transverse optical phonons of cubic ZnO in ZnO nano-tetrapods is determined by Raman spectroscopy and first-principles calculations. Stacking sequence change at the boundary of the core and legs is also identified by high-resolution transmission electron microscopy. Based on this experimental and theoretical evidence, we demonstrate that the lattice structure of ZnO nano-tetrapods is hierarchical with a zinc blende core connecting to four wurtzite legs. Furthermore, we establish the atomic configuration and propose a formation mechanism induced by Laplace pressure in the initial growth stage of ZnO nano-tetrapods.

(Some figures in this article are in colour only in the electronic version)

1. Introduction

Nano-tetrapods are regarded as promising candidates for active components in diverse technological fields due to their remarkable optical, electric and mechanical properties [1–3]. It is believed that tetrapod structures are superior in providing electron extraction to one-dimensional nanorod structures or bulk materials as interconnections and functional components in photovoltaic devices [1, 4]. ZnO tetrapods are a common morphology of ZnO, and their properties and applications have been extensively studied [5–10]. Wang *et al* reported that three-dimensional functionalized tetrapod-like ZnO nanostructures were used as novel carriers for mammalian cell transfections, which delivered plasmid DNA into the cells while standing on the cell membrane with three needle-shaped legs as a result of their tetrapodal shape [11]. Xie *et al* designed the individual ZnO tetrapod as multiterminal sensors which could simultaneously give two responses to a single outside signal at the same time to distinguish noises and increase sensitivity by comparing the intensities and directions of the two responses [12]. In recent years, owing to the requirement of device design and controlled synthesis, the lattice structure and formation mechanism of ZnO nano-tetrapods have received more and more attention. Unfortunately, although several trials were reported, the formation mechanism of ZnO tetrapods is still under debate. Up to now, there have been three different growth mechanisms to explain the formation of ZnO tetrapods. Shiojiri and Kaito reported that those particles less than 20 nm in size had the zinc blende (ZB) structure. They became tetrapod-like crystals by fast growing along four ⟨111⟩ directions perpendicular to the {111} or Zn faces. Then, wurtzite (WZ) crystals formed on their {111} faces by introducing stacking faults, and they grew along their easy growth [0001] direction to form the so-called fourings [13]. Iwanaga *et al* reported ZnO tetrapods composed of core and legs with the same WZ structure. They assumed that octahedral multiple inversion twins formed first. During their growth, cracking of some twin boundaries took place and the growth of the four legs was done only in the $+c$ directions [14, 15]. Nishio *et al* proposed a growth model that the ZnO tetrapods were formed from WZ multiple twins

[3] Author to whom any correspondence should be addressed.

induced in a ZB nucleus, and that the ZB nucleus only existed in the high-temperature tetrapods and degenerated to multiple twins at room temperature [16]. Obviously, these proposed mechanisms of ZnO tetrapods are controversial. The disputes are mainly focused on whether the ZB core exists and what is the role of the nucleus in the initial formation stage of ZnO nano-tetrapods.

To the best of our knowledge, all reported growth models of ZnO tetrapods were mainly constructed based on morphology analysis. The key limitation of the morphology observation is that just a few tetrapods can be investigated. To track the formation mechanism of ZnO nano-tetrapods, it is more effective that the microscopical results are combined with spectral measurements and theoretical calculations. Here, ZnO nano-tetrapods were synthesized by the microwave plasma method [17]. Except for the morphology analysis, Raman scattering spectroscopy was employed to characterize a large number of tetrapods, and the phonon modes of both WZ- and ZB-structured ZnO were successfully detected. By virtue of theoretical simulations, the characteristic longitudinal optical (LO) and transverse optical (TO) phonon modes of cubic ZnO in the ZnO nano-tetrapods are identified for the first time. Bringing together this credible evidence from transmission electron microscopy (TEM), Raman spectroscopy and theoretical calculations, the hierarchical lattice structure of ZnO nano-tetrapods with ZB core and WZ legs is determined. Furthermore, we establish the atomic configuration and propose a rational formation mechanism of ZnO nano-tetrapods.

2. Experimental and theoretical details

ZnO nano-tetrapods were synthesized by the microwave plasma method [17]. In a typical procedure, zinc powder in a quartz boat was set at the center (plasma heating zone) of a horizontal quartz tube. Pure Ar and O_2 gases flowed into the tube and a microwave source (800 W 2.45 kMHz) was coupled along a square rectangular wave-conducting pipe to the tube center for generating stable plasma. An assistant tube furnace was used to provide the necessary temperature zone. The as-prepared particles were collected on the inner wall at the downstream end of the tube after 30 min reaction. TEM (JEM-2000EX and -2010F, JEOL) of bright-and dark-field images, and high-resolution TEM (HRTEM) were applied to distinguish the crystal orientations and structures between the core and legs.

The phase composition was investigated at room temperature using a confocal microprobe Raman system (Renishaw UV–vis 1000) equipped with a CCD detector and a Leica DMLM microscope. The Raman spectra were excited by a 325 nm (ultraviolet) He–Cd laser, 514 nm (green) Ar+ laser and 785 nm (red) diode laser, respectively. The scattered signal was collected in a backscattering configuration through the CCD detector and fed to a spectrometer yielding a spectral resolution of <2 cm^{-1}. Because of the random alignment of nano-tetrapods, all the fundamental active modes were detected under such a optical geometry.

To verify our experiment results, further theoretical calculations were performed. The phonon dispersions were computed within the framework of the generalized gradient approximation (GGA) [18], using the plane-wave density functional theory (DFT) program ABINIT [19]. The interaction between the ions and valence electrons was described using the nonrelativistic optimized pseudopotentials [20–22]. A plane-wave basis set with 80 Hartree cutoff was used to expand the electronic wavefunctions at special k-points generated by an $(8 \times 8 \times 8)$ Monkhorst–Pack scheme. For linear response functions, the density functional perturbation theory (DFPT) was implemented to calculate the interatomic force matrices, from which phonon band structures in the Brillouin zone were obtained, with the LO–TO splitting being taken into account [19, 23].

3. Results and discussion

3.1. Microscopical observation

The bright- and dark-field images of the TEM were applied to distinguish the crystal orientations and structures between the core and legs. Figures 1(a) and (b) reveal that the ZnO nano-tetrapods consist of four straight legs with nearly uniform diameters in the range from 10 to 25 nm and lengths up to 160 nm. The dark-field image of one leg does not extend to the core, suggesting that they are impossible to satisfy the same diffraction condition. This indicates the crystal structure or orientation of the core is different from that of the legs. To gain a detailed insight, the lattice structure of the tetrapods was further investigated by HRTEM. An appropriate orientation was selected to obtain better lattice fringes of the legs, the coalescence between legs and the boundary of the core and legs, as seen in figures 1(c)–(e). Because of the relatively small sizes of oxygen atoms, only the diffraction image of zinc atoms can be clearly seen. It is shown in figure 1(c) that lattice fringes of the legs appear to be of parallel bright diffraction lines with a stacking sequence of ABAB along the perpendicular direction. The singular fringe spacing is measured to be 0.512 nm, close to the lattice constant c in hexagonal ZnO [24], implying the pure WZ-structured leg grows along the [0001] direction. The lattice difference between the core and legs makes the core region appear as a small octahedron at the joint center. From its triangle side surfaces, four equivalent WZ-structured ZnO legs grow epitaxially. Different legs are mitered by shorter parallel rows of bright dots, as denoted by the dashed lines in figure 1(d). It is seen that the miter joints are discontinuous at some regions, which suggests that the legs initially grow faster in certain crystal directions and then coalesce as they grow laterally. A remarkable feature is that the stacking sequence changes at the boundary of the core and legs. As shown in figure 1(e), the (0001) plane of the WZ leg connects with a {111} plane of the ZB structure, which indicates that the ZnO nano-tetrapod is a hierarchical structure with different lattice-structured core and legs. The core grows faster in the four equivalent crystal directions to form the four WZ-structured legs.

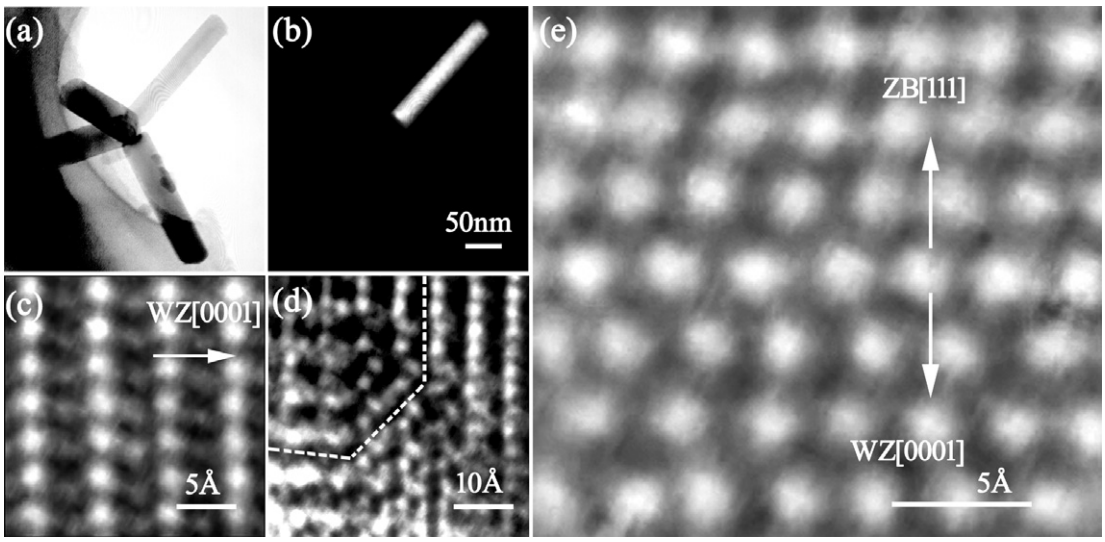

Figure 1. (a) Bright- and (b) dark-field TEM images. Typical lattice fringes of (c) the legs, (d) the coalescence between legs and (e) the boundary of core and legs observed by HRTEM.

3.2. Raman scattering spectra

Although the HRTEM images show the hierarchical lattice structure of ZnO nano-tetrapods, it could not be completely credible by just studying several tetrapods. Here, Raman spectroscopy was employed to investigate a large quantity of ZnO nano-tetrapods, as shown in figure 2, which were taken at room temperature by three different excitation sources. The peaks located at 380, 410, 439, 570 and 587 cm^{-1} in figures 2(a) and (b), respectively, correspond to the A_1(TO), E_1(TO), E_2(high), A_1(LO) and E_1(LO) phonon modes of WZ ZnO [24–27]. In particular, the A_1(TO) mode, which is difficult to obtain due to the destructive interference between the Fröhlich interaction and the deformation-potential contributions to the LO-phonon scattering, is also present in our Raman results [24]. For the WZ phase, the optical phonon modes at the Brillouin zone center Γ could be classified according to the irreducible representations of the point group C_{6v}. The modes A_1, E_1 and E_2 are Raman-active while the B_1 mode is not [24, 28]. The E_1 mode splits into TO and LO components caused by the macroscopic electric fields, and the A_1 branch shows different frequencies when approaching the Γ-point from different symmetry directions, thus splitting also into TO and LO modes [24, 29]. In addition, the peaks at the frequencies 331 and 541 cm^{-1} have been assigned to second-order Raman spectra of the WZ phase [24]. Owing to the shorter laser wavelength, most of the low-frequency signals are buried in the noise when measured by the 325 nm He–Cd laser in figure 2(c). Except for the predominant WZ ZnO phonons, there are two obvious peaks appearing at 399 and 581 cm^{-1}. The former is present between WZ A_1(TO) and E_1(TO) modes, and the latter is detected between WZ A_1(LO) and E_1(LO) modes. However, they do not belong to any characteristic spectrum of the WZ phase.

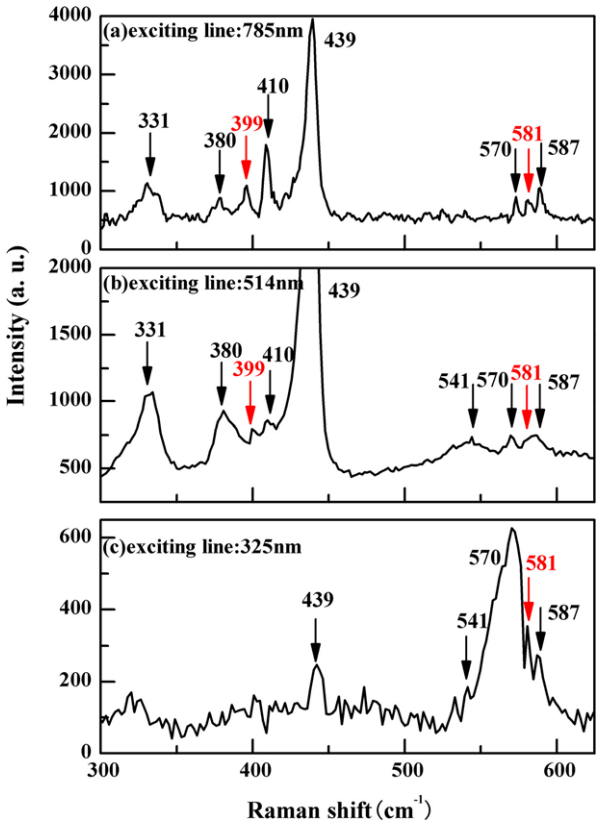

Figure 2. Raman spectra of the ZnO nano-tetrapods, taken by (a) 325 nm, (b) 514 nm and (c) 785 nm exciting sources, respectively.

3.3. Phonon dispersion relations

According to the structural information in the typical HRTEM images, the ZB structure as the core of ZnO nano-tetrapods is preferable. In order to further identify the two additional Raman peaks, the phonon dispersion curves for both the WZ and ZB structures were calculated, as displayed in figure 3. The WZ-structured ZnO has four atoms (two zinc and two oxygen atoms) per unit cell, leading to twelve phonon modes, nine optical and three acoustic branches. Whereas in the

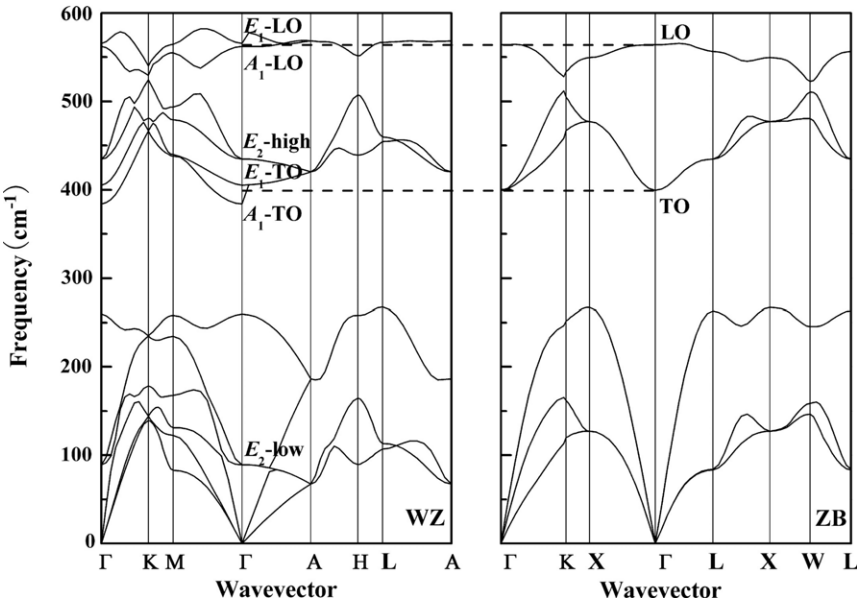

Figure 3. First-principles calculated phonon dispersion curves of WZ-and ZB-structured ZnO.

ZB primitive unit cell, there are two atoms (one zinc and one oxygen atoms), giving only six phonon modes, three of which are acoustical and the others are optical branches [30]. Moreover, the ZB phase belongs to the tetrahedron point group, having one optical phonon mode at the Γ-point. The optical phonon mode splits into TO and LO modes due to the symmetry of the three-dimensional (3D) irreducible representation T_2 [29]. A more distinct fingerprint of the phase structure is provided by comparing the calculated Γ-point frequencies with the experimental data. The theoretical TO phonon frequency agrees very well with the low-frequency 399 cm^{-1} peak, although there is some deviation for the LO mode. The deviation is derived from the semiempirical models in *ab initio* lattice dynamics calculations, which usually underestimate the high-frequency LO mode in the ZB phase [30]. A similar underestimate happens in the E_1(LO) and A_1(LO) phonon frequencies. However, the phonon relations between the two modifications still hold. It is known that the atomic arrangements of the two modifications are quite similar except for the angle of adjacent tetrahedral units, which is 0 for the WZ and 60° for the ZB phase. The WZ structure can be treated as arising from the ZB one by compressing the crystal and changing the stacking of layers along the ⟨111⟩ axis [31]. The compression results in the crystal field that makes the T_2 mode of the cubic phase split off into the A_1 and E_1 modes of the anisotropic hexagonal crystal. Hence, the cubic TO mode is generally located between hexagonal A_1(TO) and E_1(TO), and the LO mode is located between hexagonal A_1(LO) and E_1(LO) modes at Γ-point [28], as labeled with the broken lines. This relation is generally consistent with our observation that the 399 cm^{-1} occurs between WZ A_1(TO) and E_1(TO), and the 581 cm^{-1} lies between WZ A_1(LO) and E_1(LO) phonons. Therefore, the two peaks are speculated to be derived from the TO and LO phonons of ZB ZnO, respectively. Although the TO mode is nominally forbidden, it becomes allowed due to any short range perturbations in the lattice structures [28]. The appearance of both the TO and LO phonons in the three Raman spectra further supports the microscopical results, and indicates that the ZB phase exists widely in ZnO nano-tetrapods.

3.4. Atomic configuration

The appearance of both the TO and LO phonons in the Raman spectra demonstrates the existence of a ZB phase in ZnO nano-tetrapods. HRTEM observation suggests the four legs of the tetrapods are pure WZ phase, so the ZB phase must exist in the core. To form the tetrapod-like crystals, the core should have four equivalent planes which match the (0001) plane of the WZ structure. Considering the lattice symmetry, the core with WZ structure has only two equivalent planes ((0001) and $(000\bar{1})$) which are impossible to form the four legs unless lattice defects, such as multiple twins, are induced [14–16]. However, the defects are not observed in all our HRTEM images of the core. In contrast, the octahedral ZB crystal has four equivalent planes {111}. The atomic arrangements in these planes are quite similar to those of the (0001) plane in the WZ type except for the stacking sequence difference. Bringing together these results, the ZB-structured core emerged and the hierarchical structure of ZnO nano-tetrapods with ZB core and WZ legs is determined. To shed light on the origin, the atomic configuration of ZnO nano-tetrapods is established schematically in figure 4. As a result of the self-catalysis effect of the cation-terminated surfaces, the four positive charged surfaces ((111), $(\bar{1}\bar{1}1)$, $(1\bar{1}\bar{1})$ and $(\bar{1}1\bar{1})$) of the octahedral ZB core serve as the fast growth fronts. The WZ crystals grow on these faces by introducing stacking faults to form the four equivalent legs, just as in the TEM image in figure 1(a). Figure 4(b) shows the boundary of the core and two legs. From this perspective, the Zn–O bilayers in the legs appear to be of parallel lines. The stacking sequence changes from AB to ABC during the phase transformation from the leg

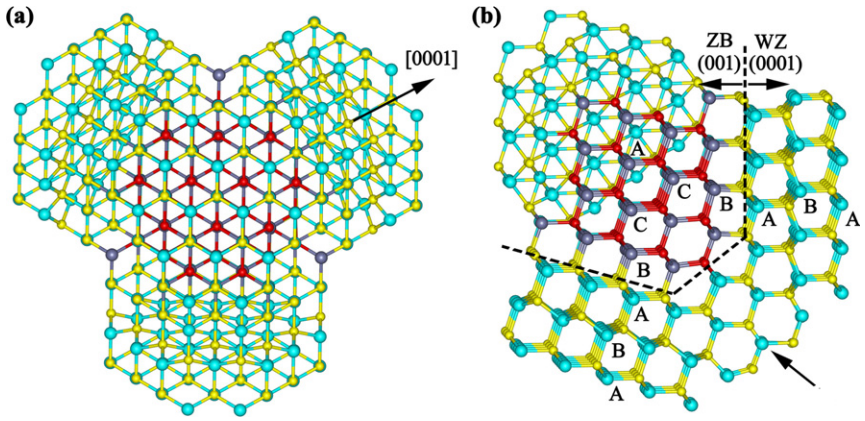

Figure 4. The lattice models of ZnO nano-tetrapods: (a) a view from the tail of one leg and (b) the boundary of the core and two legs. The dark- and light-colored large balls represent the zinc atoms in the core and legs, respectively. The dark- and light-colored small balls represent the oxygen atoms in the core and legs, respectively.

to the core. The parallel lines of adjacent legs are mitered by shorter parallel rows around the core, as denoted by the dashed lines. Since the four WZ-type legs have different orientations, the bonds for an atom between the adjacent legs are on a plane instead of tetrahedral bonds, as marked by the arrow in figure 4(b). It is presumably responsible for the discontinuity of the miter joints at some regions. All these structural characteristics are consistent with the information from HRTEM images in figures 1(c)–(e), demonstrating the rationality of the constructed atomic configuration of ZnO nano-tetrapods.

3.5. Formation mechanism

It is well known that bulk ZnO crystallizes only in the stable hexagonal WZ phase under ordinary conditions because its ionicity resides at the borderline between covalent and ionic materials [31]. Interestingly, the hierarchical model of ZnO nano-tetrapods has both the WZ and ZB phases. There must be a feasible formation mechanism reversing the stability of the two phases during the growth. A very common growth mode of thin films is the Volmer–Weber mode involving three growth stages: the isolated 3D islands nucleate and grow, then these islands merge and percolate and the remaining channels are filled. Then subsequently a continuous film grows [32, 33]. It has been found that an intrinsic compressive stress (i.e. Laplace pressure) induced by the surface tension exists in many isolated 3D islands in Volmer–Weber growth [34–36]. In light of this, small structures are subjected to a stressed state even without any external force. On the assumption that an isolated particle is a pellet, the Laplace pressure is determined by the radius r. Its magnitude can be estimated by the Laplace formula $P_{\text{Laplace}} = 4\sigma r^{-1}$, where σ is the surface stress with its sign depending on the surface stress being tensile or compressive [37]. When the core starts to grow, the particle size is small enough that P_{Laplace} can be estimated to exceed 20 GPa if σ is only larger than 10 N m^{-1} for ZnO (it has been reported that σ is up to 40 N m^{-1} in some materials [32]). As we have predicted [38], under such a large compressive pressure, the ZB phase is more stable on account of its lower Gibbs free energy than that of the WZ phase. The hierarchical ZnO nano-tetrapods are believed to originate from small particles, in which the ZB structure is preferable [38]. As the particles grow, the increasing radius r results in the reduction of P_{Laplace} and thus raises the Gibbs free energy of the ZB phase. When the particle size exceeds the critical value, the WZ phase has lower Gibbs free energy instead, so a phase transition happens and the four legs turn out to be the WZ structure at this crystal growth stage. Meanwhile, an energy barrier has arisen from the growth in the four equivalent orientations, which prevents the ZB core from transforming into the WZ phase.

4. Conclusions

In summary, the hierarchical lattice structure of ZnO nano-tetrapods with ZB core and WZ legs is demonstrated by means of microscopical analysis, Raman spectroscopy and theoretical calculations. Crystal orientation or structure of the legs is imaged to be different from that of the core in dark-field TEM. The stacking sequence change during the phase transformation could be clearly observed at the boundary of the core and legs in HRTEM images. Raman spectroscopy was employed to study a large number of ZnO nano-tetrapods. To our knowledge, this is the first time that the ZB phase has been detected in ZnO nano-tetrapods by the combination of Raman spectra and the first-principles calculated phonon dispersion relations. Based on these results and the considered lattice symmetry, the atomic configuration of ZnO nano-tetrapods is constructed with one ZB core connecting to four WZ legs, which is coincident with the HRTEM images. Furthermore, the formation mechanism induced by Laplace pressure in the initial growth stage of ZnO nano-tetrapods is proposed.

Acknowledgments

We acknowledge assistance from Mr Wei Lin, Changjie Zhou and Wei Jiang. This work was supported by the National Natural Science Funds (60827004 and 60776066), and the Science and Technology Programs of Xiamen and Fujian of China.

References

[1] Zhang Z *et al* 2007 *Appl. Phys. Lett.* **90** 153116
[2] Leung Y H, Kwok W M, Djurišić A B, Phillips D L and Chan W K 2005 *Nanotechnology* **16** 579
[3] Djurišić A B, Kwok W M, Leung Y H, Chan W K, Phillips D L, Lin M S and Gwo S 2006 *Nanotechnology* **17** 244
[4] Newton M C and Warburton P A 2007 *Mater. Today* **10** 50
[5] Kitano M, Hamabe T and Maeda S 1990 *J. Cryst. Growth* **102** 965
[6] Yan H Q, He R R, Pham J and Yang P D 2003 *Adv. Mater.* **15** 402
[7] Chen Z, Shan Z W, Cao M S, Lu L and Mao S X 2004 *Nanotechnology* **15** 365
[8] Djurišić A B, Choy W C H, Roy V A L, Leung Y H, Kwong C Y, Cheah K W, Gundu Rao T K, Chan W K, Lui H F and Surya C 2004 *Adv. Funct. Mater.* **14** 856
[9] Zhang J, Yang Y, Xu B, Jiang F and Li J 2005 *J. Cryst. Growth* **280** 509
[10] Fischer A M, Srinivasan S, Garcia R, Ponce F A, Guaño S E, Di Lello B C, Moura F J and Solórzano I G 2007 *Appl. Phys. Lett.* **91** 121905
[11] Nie L, Gao L, Feng P, Zhang J, Fu X, Liu Y, Yan X and Wang T 2006 *Small* **2** 621
[12] Zhang Z, Sun L, Zhao Y, Liu Z, Liu D, Cao L, Zou B, Zhou W, Gu C and Xie S 2008 *Nano Lett.* **8** 652
[13] Shiojiri M and Kaito C 1981 *J. Cryst. Growth* **52** 173
[14] Fujii M, Iwanaga H, Ichihara M and Takeuch S 1993 *J. Cryst. Growth* **128** 1095
[15] Iwanaga H, Fujii M and Takeuchi S 1993 *J. Cryst. Growth* **134** 275
[16] Nishio K, Isshiki T, Kitano M and Shiojiri M 1997 *Phil. Mag.* A **76** 889
[17] Zhang X H, Xie S Y, Jiang Z Y, Xie Z X, Huang R B, Zheng L S, Kang J Y and Sekiguchi T 2003 *J. Solid State Chem.* **173** 109
[18] Jaffe J E, Snyder J A, Lin Z and Hess A C 2000 *Phys. Rev.* B **62** 1660
[19] Gonze X *et al* 2005 *Z. Kristallogr.* **220** 558
[20] Li C, Guo W, Kong Y and Gao H 2007 *Phys. Rev.* B **76** 035322
[21] Qteish A 2000 *J. Phys.: Condens. Matter* **12** 5639
[22] Hill N A and Waghmare U 2000 *Phys. Rev.* B **62** 8802
[23] Saib S, Bouarissa N, Rodríguez-Hernández P and Muñoz A 2008 *J. Appl. Phys.* **103** 013506
[24] Özgür Ü, Alivov Y I, Liu C, Teke A, Reshchikov M A, Doğan S, Avrutin V, Cho S-J and Morkoçd H 2005 *J. Appl. Phys.* **98** 041301
[25] Tabata A, Enderlein R, Leite J R, da Silva S W, Galzerani J C, Schikora D, Kloidt M and Lischka K 1996 *J. Appl. Phys.* **79** 4137
[26] Serrano J, Manjón F J, Romero A H, Ivanov A, Lauck R, Cardona M and Krisch M 2007 *Phys. Status Solidi* b **244** 1478
[27] Koyano M, Quocbao P, Thanhbinh L T, Hongha L, Ngoclong N and Katayama S 2002 *Phys. Status Solidi* a **193** 125
[28] Alim K A, Fonoberov V A and Balandin A A 2005 *Appl. Phys. Lett.* **86** 053103
[29] Serrano J, Romero A H, Manjón F J, Lauck R, Cardona M and Rubio A 2004 *Phys. Rev.* B **69** 094306
[30] Siegel A, Parlinski K and Wdowik U D 2006 *Phys. Rev.* B **74** 104116
[31] Ashrafi A and Jagadish C 2007 *J. Appl. Phys.* **102** 071101
[32] Koch R, Hu D and Das A K 2005 *Phys. Rev. Lett.* **94** 146101
[33] Floro J A, Kotula P G, Seel S C and Srolovitz D J 2003 *Phys. Rev. Lett.* **91** 096101
[34] Wang X-S, Kushvaha S S, Yan Z and Xiao W 2006 *Appl. Phys. Lett.* **88** 233105
[35] Mayr S G and Samwer K 2001 *Phys. Rev. Lett.* **87** 036105
[36] Pao C W and Srolovitz D J 2006 *Phys. Rev. Lett.* **96** 186103
[37] Spaepen F 2000 *Acta Mater.* **48** 31
[38] Wu Y, Kang J and Liu F 2008 *J. Mater. Res.* **23** 3347